

This is an Open Access document downloaded from ORCA, Cardiff University's institutional repository:<https://orca.cardiff.ac.uk/id/eprint/146826/>

This is the author's version of a work that was submitted to / accepted for publication.

Citation for final published version:

Prato, A., Al-Saymaree, M. S. M., Featherston, C. A. and Kennedy, D. 2022. Buckling and post-buckling of thin-walled stiffened panels: modelling imperfections and joints. *Thin-Walled Structures* 172 , 108938. 10.1016/j.tws.2022.108938

Publishers page: <https://doi.org/10.1016/j.tws.2022.108938>

Please note:

Changes made as a result of publishing processes such as copy-editing, formatting and page numbers may not be reflected in this version. For the definitive version of this publication, please refer to the published source. You are advised to consult the publisher's version if you wish to cite this paper.

This version is being made available in accordance with publisher policies. See <http://orca.cf.ac.uk/policies.html> for usage policies. Copyright and moral rights for publications made available in ORCA are retained by the copyright holders.



Buckling and post-buckling of thin-walled stiffened panels: modelling imperfections and joints.

A. Prato^a, M.S.M. Al-Saymaree^a, C.A. Featherston^{a1}, D. Kennedy^a

^a Cardiff University, School of Engineering,
Queen's Buildings, The Parade, Cardiff, CF24 3AA, UK

Abstract

This paper explores the effect of different modelling strategies to represent geometrical imperfections and joints in flat thin-walled stiffened panels during buckling and post-buckling. Compression tests were performed on aircraft grade aluminium alloy panels jointed to L-shape stiffeners using rivets with digital image correlation used to monitor out-of-plane deformations, mode shape changes and failures such as stiffener debonding. Experiments were replicated using finite element analysis employing different levels of complexity to model geometric imperfections and joints. The advantages and limitations of these strategies are discussed and recommendations are made.

Keywords: Thin-walled structures, Stiffened panels, Buckling, Geometrical imperfections and joints, Digital Image Correlation (DIC), Finite Elements (FE)

Introduction

Thin-walled structures are some of the most efficient structures available having high specific stiffness and strength. One of the most commonly used is a stiffened panel, a thin skin reinforced using prismatic stiffeners although more recently innovative topologically optimised stiffened structures designed using different numerical modelling approaches are beginning to be explored. For example, Balabanov and Haftka investigated how the wing-fuselage interaction, and in particular the fuselage flexibility, can influence the topology of the internal structure of a wing of a high-speed civil aircraft [1]. Dunning et al. [2] proposed a new design for a wing box using the level-set method for topology optimization and Aage et al. presented a giga-voxel morphogenesis methodology used to design and optimise an aircraft wing structure [3].

Due to the high computational cost of some of these optimisations, and difficulties manufacturing the resulting geometries, stiffened panels are at present still widely used and therefore of great interest in sectors such aerospace and civil engineering. However their performance can be significantly affected by

1 Corresponding author
Email address: featherstonca@cardiff.ac.uk

geometric and loading imperfections which must therefore be taken into account when finalising designs and choosing appropriate safety factors. Localised small geometrical imperfections in metal components or barely visible damage (BVID) in composites, can lead to significantly reduced buckling loads and unstable behaviour resulting in catastrophic failures. Premature failures can also be caused by localised overloading/pre-cracks resulting from pre-existing small imperfections [4-6], related to manufacturing processes (e.g. the use of rivets and local misalignments of structural components) or to material defects (e.g. dislocation planes, pre-cracks). The latter is particularly relevant for stiffened panels, which are often manufactured by connecting the stiffeners and the skin using rivets. Extensive work therefore has been completed in order to quantify the effect of these imperfections, resulting for example in Knock Down factors which can be applied to theoretical loads. This began with the building of extensive data banks [7] for different loading and boundary conditions but more recently has been achieved using finite element analysis and numerical modelling [8-11]. A recent review of experimental and numerical studies of axially compressed curved panels was carried out by Martins et al. [12].

Ideally, FEA models use data on the geometrical imperfections present in a structure based on measurements from individual components but this is not always available and a number of practices such as the introduction of eigenmode shaped imperfections scaled to represent the amplitude of the imperfections present have been adopted. The results obtained however, can be highly sensitive to the level of sophistication of the models created [13, 14]. This is particularly true for example with respect to the curvature [15, 16], the geometry of the imperfection [17, 18], the boundary conditions [19] or the complexity of the model in relation to the behaviour of any fasteners holding the skin and stiffeners together. This should be balanced with the level of computational effort required to process these models.

In the research presented here the effect of the presence of joints and geometric imperfections, no material imperfections considered, on the buckling and post-buckling of thin-walled stiffened panels, is observed in experimental tests using Digital Image Correlation (DIC) [20] to create out-of-plane displacement data and strain distribution maps. Finite element models with varying degrees of sophistication, are then created and recommendations made on their suitability based on comparison to the experimental results.

Materials and methods

Materials

Aluminium alloy 6082-T6 was used to manufacture the skin and stiffeners of the panels tested. Two tensile test specimens were cut from both the skin and stiffener materials to determine the mechanical properties for each component in accordance with the British Standard BS EN ISO 6892-1-2016 [21]. The geometry and nominal dimensions of these specimens are provided in Figure 1 and Table 1.

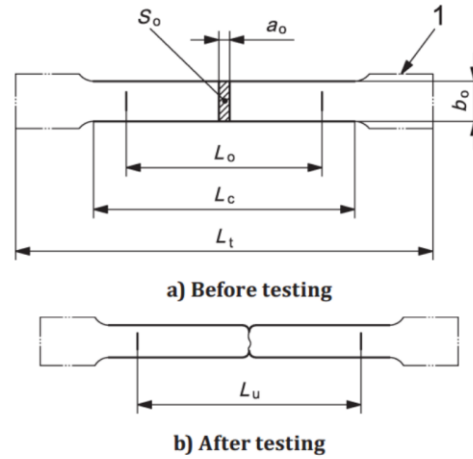


Figure 1: Tensile test specimen geometry [21]

	a_o	b_o	r	L_o	L_c	L_t
Standard						
Type 1 - <i>mm</i>	< 3.0	12.5 ± 1	≥ 20.0	50	57 ≤ L_c ≤ 75	> 87.5
Type 2 - <i>mm</i>	< 3.0	20.0 ± 1	≥ 20.0	50	62.5	205
Type 3 - <i>mm</i>	< 3.0	25.0 ± 1	≥ 20.0	50	-	
Experimental test						
Skin panel spec. - <i>mm</i>	1.0	12.5	25	50	62.5	205
Stiffeners spec. - <i>mm</i>	1.5	12.5	25	50	62.5	205

Table 1: Tensile specimen dimensions: standard [21] and experimental tests.

where a_o is the specimen thickness, b_o the specimen width, r the transition radius, L_o the original gauge length, L_c the parallel length and L_t the total length.

Tensile tests were carried out using a Zwick/Roell Z100 100 kN load cell mechanical testing machine [22] at a crosshead displacement rate of 0.15 mm/min. An extensometer was used to measure the local linear strain data at the centre of the specimens. Figure 2 shows the tensile test results in terms of stress-strain curves. Table 2 presents the main material data and mechanical properties. Failure occurred in all the specimens close to the middle of the gauge length, in accordance with the failure mode proposed in [21].

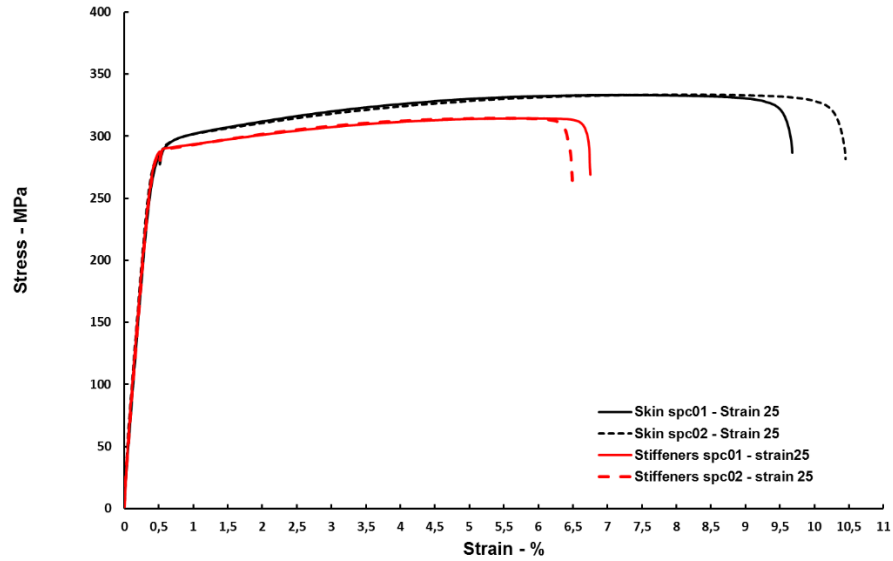


Figure 2: Tensile test experimental results

	Skin	Stiffeners
Density (**) - kg/m^3	2700	2700
Elastic modulus (*) - GPa	72.2	72.6
Poisson's ratio -	0.3	0.3
Tensile strength (*) - MPa	333.0	314.5
Yield stress (*) - MPa	285.9	287.4
Strain at yield stress (*) - %	0.51	0.51
Stress at failure (*) - MPa	286.6	266.8
Strain at failure (*) - %	9.68	6.62

Table 2: Aluminium alloy 6082-T6 properties: (*) average values as from experimental tests, (**) from datasheet [23, 24].

As the results were consistent, and to minimize material consumption, no additional specimens were produced for these tests and the mechanical properties obtained were used in the numerical material models.

Experimental tests: methodology overview

Stiffened panels

Two flat thin-walled panels were manufactured. The stiffened-panels' skins, 430mm long and 400mm in width, were produced from a 1mm thick aluminium alloy 6082-T6 flat sheet.

The L-shape stiffeners, 430mm long, 20 mm wide, 50 mm high and 1.5 mm thick, were made from 6082-T6 aluminium alloy angle extruded bar with an initial width of 50 mm. Each stiffened panel had five stiffeners, whose distribution along the panel width is shown in Figure 3.

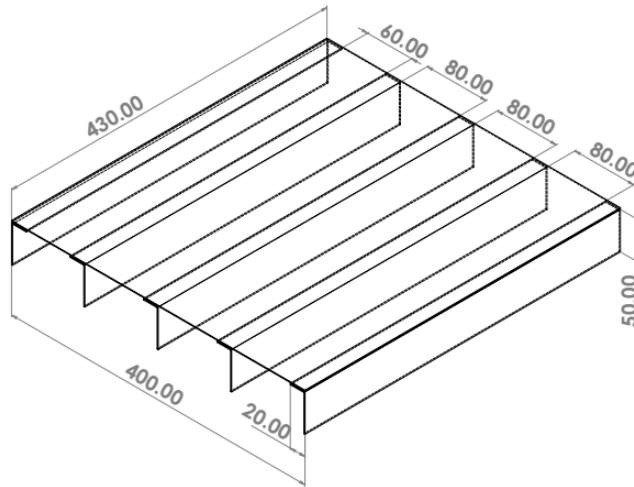


Figure 3: CAD model of the flat stiffened panels: stiffeners location and distribution along the skin width. All the dimensions are in mm.

To join the structural components together, a thin layer of Loctite Multi-bond 330 adhesive [25], see Table 3, and 75 stainless steel rivets, 15 for each stiffener, were used. Rivet holes were drilled during the skin and stiffeners' manufacture at a spacing of 25mm with the components joined together afterwards to produce the stiffened panels.

Loctite Multi-bond 330 adhesive [26]	
<i>Typical properties of uncured material:</i>	
Specific Gravity @ 25 °C	1.05
Viscosity @ 25 °C - mPa·s	30,000 to 70,000
<i>Typical properties of cured material:</i>	
Coefficient of Thermal Expansion - K^{-1}	8×10^{-6}
Coefficient of Thermal Conductivity - $W/(m \cdot K)$	0.1
Specific Heat - $kJ/(kg \cdot K)$	286.6
<i>Typical performance of cured material (after 24 hours @ 22 °C):</i>	
Lap Shear strength: mild steel - N/mm^2	15 to 30
Tensile strength: mild steel - N/mm^2	12 to 22
<i>Typical environmental resistance (cured for 1 week @ 22 °C_i):</i>	
Lap Shear strength: mild steel - mm (gap)	0.25

Table 3: Loctite Multi-bond 330 adhesive properties from datasheet [29].

Geometrical imperfections in the form of differences between the stiffener and skin lengths (in-plane) with the stiffener being longer in each case were noted and measured using a depth gauge. The average measured values of these differences in length were equal to 0.5 mm in Stiffener 03, 0.4 mm in Stiffener 04 and 0.5 mm in Stiffener 05 respectively, see Figure 4. Out-of-plane imperfections were also seen, with a maximum amplitude in the order of 2.0-3.0 mm from the DIC before the beginning of the debonding and failure in the structures.

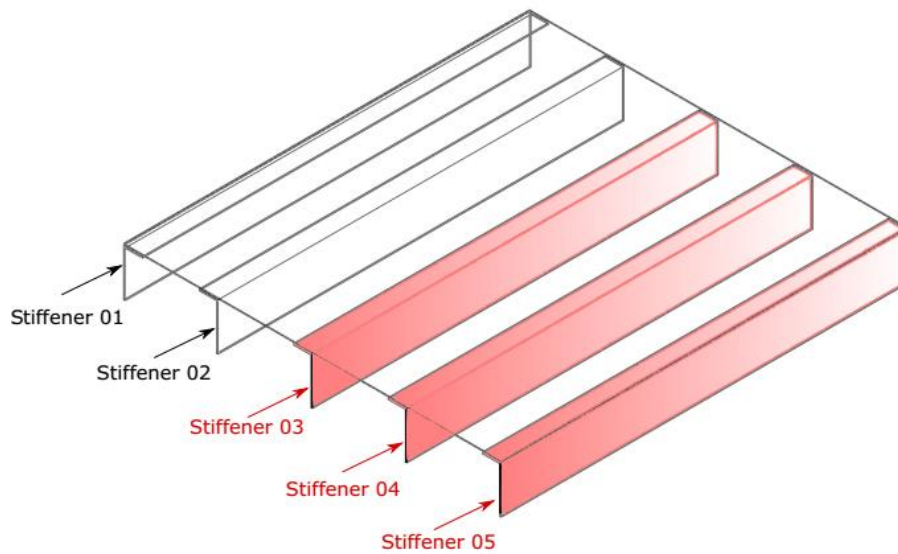


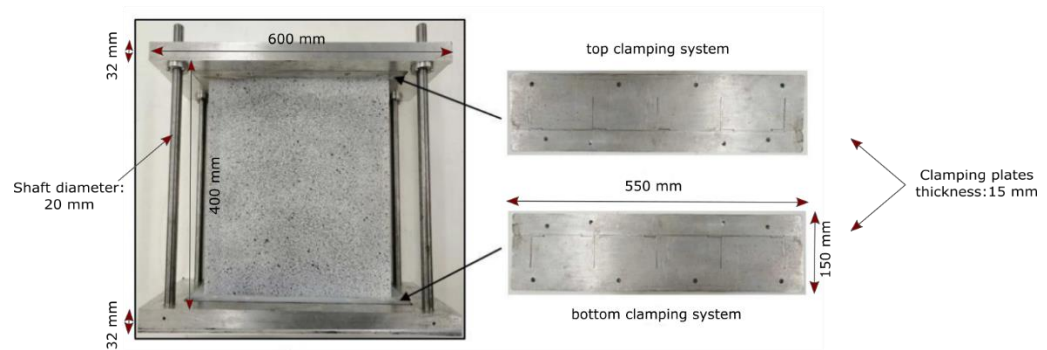
Figure 4: Location of geometric imperfections.

These in-plane and out-of-plane geometric imperfections were represented in the model along with detailed models of the joints.

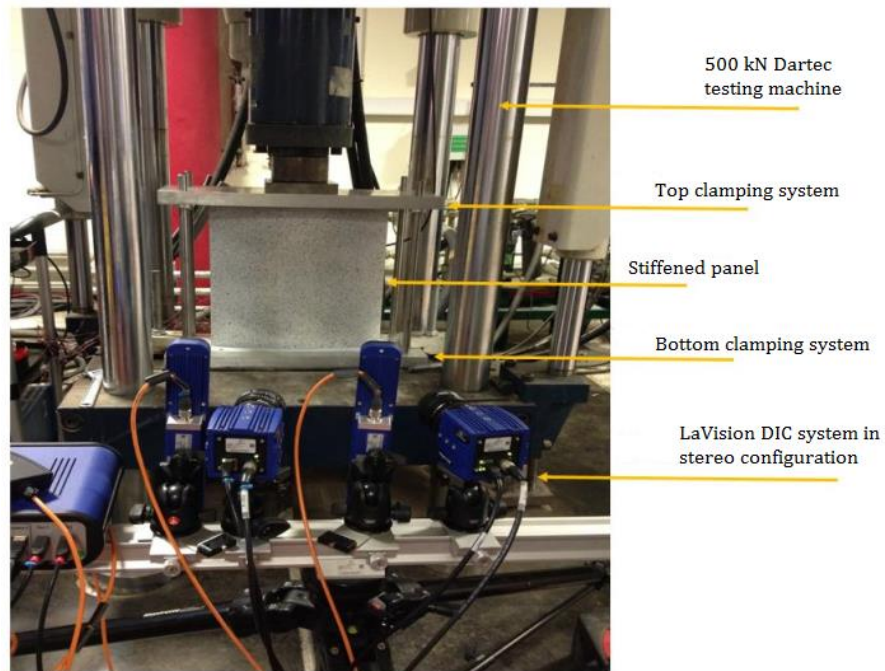
Buckling tests

Compression tests on the stiffened panels were performed using a 500 kN Dartec servo-hydraulic testing machine [22] at a crosshead displacement rate of 0.15mm/min.

To provide built-in boundary conditions along the top and bottom edges, a bespoke system was designed and manufactured, see Figure 5 (a), to prevent rotation and displacement of the bottom edge, and allow only vertical displacement of the top edge. This was achieved by clamping each end of the specimen between two plates, 15mm thick, machined to create the required profile to contain the skin and stiffeners, with shims to fill any gaps between the specimens and the clamps. Each of these pairs of clamps was then fitted into a machined recess and bolted to either the top or bottom plate of the rig, to secure the specimen in place.



(a)



(b)

Figure 5: (a) Bespoke clamping system and (b) experimental tests main setup.

To track the strain distribution during the tests, an 8MP LaVision system [20] was used in stereo configuration to perform a Stereo DIC [26-28] and collect data on the out-of-plane displacement of the skin, see Figure 5 (b). A speckle pattern was used to track the skin shape changes. Table 4 presents the main setup and processing parameters used for the DIC analysis.

Characteristic	Set-Up
Technique used	Stereo DIC
Software	DaVis 8.0
Subset size (pixels)	125 x 125
Step size (pixels)	31
Camera	Imager X-light 8MP
Lens	Hama 24mm f/1-2.8D
Sampling rate (MHz)	0.25
Image Resolution (pixels)	3312 (w) × 2488 (h)
Field of view (mm)	364.5 (w) × 273.4 (h)
Focal length (mm)	54.9
Spatial resolution (mm)	3.4

Table 4: Stereo DIC set-up and processing parameters.

The force-displacement curves obtained from the Dartec test machine and the out-of-plane displacements from the DIC output were used to compare the stiffened panels' responses.

2.3 Numerical models: methodology overview

Numerical finite element (FE) models of the experimental buckling tests were developed in ABAQUS [29]. Both in-plane (due to differences in length between the skin and stiffeners) and out-of-plane geometric imperfections were introduced. A single-component model (integrating both the skin and stiffeners) was compared with a multi-component structure (in which the skin and stiffeners were modelled separately with appropriate joints) to study the effect of the presence of imperfections and joints. Only the region of interest, between the clamps (400mm long, 400mm wide and 50mm high), was considered.

The stiffened panels were modelled using linear quadrilateral general purpose shell elements of type S4R [30] with a nominal dimension of 2.5mm and 5 integration points through the thickness, for both the skin and the stiffener components. A parametric study on mesh sensitivity was presented in a previous study [31] to optimise the computational time and the results.

Material properties were defined in accordance with the experimental tensile test results for the elastic and plastic behaviour, see Table 2 and Figure 2.

Imperfections were introduced using two different strategies for the in-plane and out-of-plane strategies. First in-plane imperfections due to differences in the lengths of the stiffeners and the skins leading to uneven load distribution were modelled directly based on the measurements given in the "Stiffened Panel" section. A localised initial displacement was imposed in correspondence of the stiffeners where these imperfections were measured. Then out-of-plane imperfections, based on modes 1, 2 and 6 from the buckling analysis were introduced, see Figure 6. These modes were selected based on those seen during post buckling as the panel undergoes mode jumping and the initial three half wavelength mode seen at the point of buckling changes to a four-half wavelength mode. These are scaled (0.25mm, 0.2mm, 0.15mm) to seed the order that they

appear whilst giving a maximum amplitude equal to that found in the panels tested.

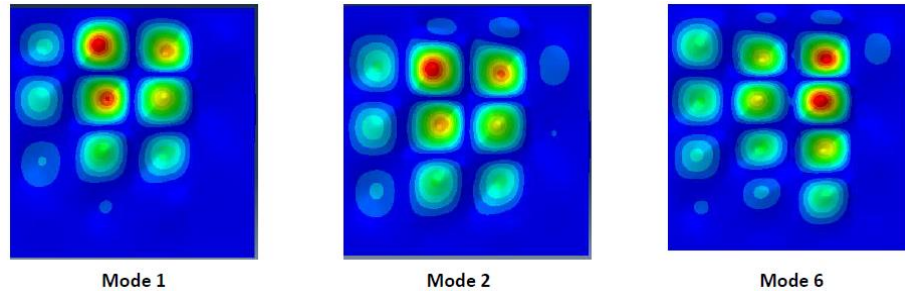


Figure 6: Three LB modes considering in the definition of imperfections.

In the single-component model, three different regions of interest, and related sections, were defined: the skin only region (1.0 mm thick with skin material properties), the stiffener only region (1.5 mm thick with stiffener material properties) and the jointed region (2.5 mm thick with hybrid material properties, modelled as the weighted ratio between the skin and stiffener experimental material properties). In the multiple-component model, in which the skin and the stiffeners were designed separately, each was assigned the appropriate material properties and sections.

In the multi-component model, as the stiffeners were connected to the skin using rivets, discrete node-based elements were used to simulate the joints. The location of the numerical rivets was the same as the physical elements. Moreover, as the rivets contribute 11% of the overall mass of the structure, (where the total mass of the stiffened panel is equal to 1.11 kg), point masses were added locally to correspond to the rivets to ensure this effect was taken into consideration (especially in the non-linear explicit analysis). The possibility of using cohesive elements to simulate the adhesive was initially considered. From results obtained using a simplified preliminary model, the contribution of the cohesive elements appeared to be negligible when compared to the effect of the rivets in terms of the force/displacement curve. In contrast, the computational cost was increased by approximately 30%. They were not therefore used in the final models proposed to reduce the computational cost.

Surface-to-surface contacts (Figure 7) were used to correctly define the interactions between the skin and stiffeners avoiding co-penetration due to differences in local deformation between the structural components, whilst allowing them to separate and thus more accurately model collapse.

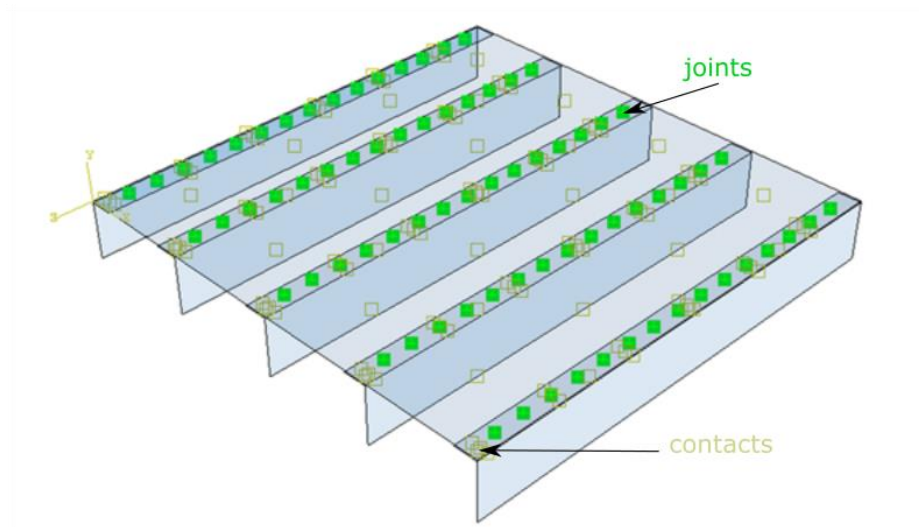


Figure 7: Numerical model of the flat panel, including discrete joints, with related local masses (green) and contacts (light brown).

In accordance with the experimental tests, see Figure 5, the ends of the panel, orthogonal to the stiffeners' cross-section, were subjected to boundary conditions representing the clamping system. The bottom edge was modelled as fixed whilst along the top edge only displacement in the loading direction was permitted to allow the compression of the panel.

A two-stage analysis was performed, a linear buckling analysis to derive the buckling modes, followed by a nonlinear analysis, i.e. geometrically nonlinear imperfections analysis with included a nonlinear material model for aluminium alloy, accordingly with experimental data, see "Materials" section, to investigate the effect of the imperfections.

In the LB study, a two-step analysis was performed:

- Initial step: boundary conditions imposed
- Step-1: LB analysis with application of the loading condition, modelled as an applied force distributed over the loading edge, including both stiffener and skin edges.

In the NLB study, three-steps were used:

- Initial step: boundary conditions imposed
- Step-1: in-plane and out of plane imperfections introduced. Three modes from the LB analysis, see Figure 6, were superposed to define the out-of-plane imperfections,
- Step-2: the load was applied under displacement control, in accordance with the experimental tests.

Five simulations were carried out for both single-component and the multi-component structures to explore the effect of different imperfections and joints:

- Stiffened panel with in-plane and out-of-plane imperfections
- Stiffened panel with out-of-plane imperfections only
- Stiffened panel with out-of-plane imperfections and in-plane imperfections only on Stiffener 5
- Stiffened panel with out-of-plane imperfections and in-plane imperfections only on Stiffener 4
- Stiffened panel with out-of-plane imperfections and in-plane imperfections only on Stiffener 3

Results

The force-displacement curves and out-of-plane displacement plots are presented in this section for both the experimental tests and the FE analysis for the multi-component model with joints and all in-plane and out-of-plane imperfections.

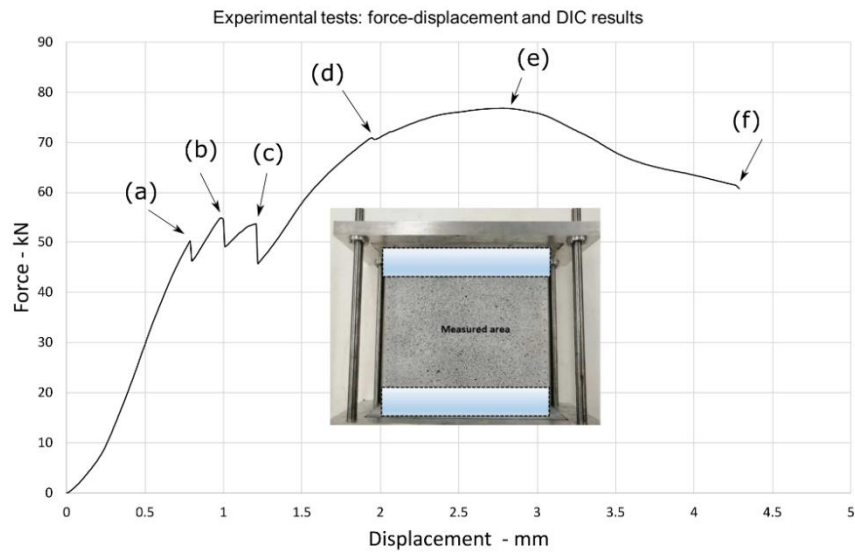
Results from the other numerical models, including different geometrical imperfections and joint modelling strategies are introduced in the discussion.

Experimental tests

Figures 8 and 9 show the force-displacement curves and out-of-plane displacement plots for test Panel 1 and Panel 2 respectively. In both cases, an initial non-linear response is seen, which is caused by the structure settling into the clamping system. Moreover, there are significant differences in the structural responses between the two panels, both in the linear and nonlinear, plastic response. For Panel 1, the force-displacement curve, after an initial linear elastic response, shows three peaks followed by drops in load of around 50 kN, corresponding to changes in buckling mode, in the left hand area between the stiffeners in Figure 8 (a) and (b). The following nonlinear behaviour corresponding to a further increase in force leads to a peak at 76.8 kN with a crosshead displacement equal to 2.8 mm. Panel 2 however, after an initial linear elastic response, continues to carry an increasing level of load until it reaches a peak force of 85 kN, after which jumps in force-displacement curve are seen as the damage in the structure progresses.

Images obtained using DIC in Stereo configuration, representing the out-of-plane displacement response, show that both Panel 1 and Panel 2 switch from mode 3 to mode 4 and then to mode 5 as loading progresses. They also show local damage around the joint between the stiffener and the skin in the upper section of stiffener three has led to a lack of support and the local deformation of the panel which is confirmed in Figure 9. This change is particularly noticeable when comparing images (c) and (d) to image (e) with buckles initially constrained to the unsupported regions between the second and third and third

and fourth stiffeners joining together due to the lack of support in the stiffener area which is accompanied by a drop in the supported load. The maximum displacement measured during the tests before interrupting them for safety reasons and indicated by the red contour, was 15 mm for Panel 1 and of 9.5 mm for Panel 2 where the stiffener has debonded. This eventually leads to the failure of the panel as shown in Figure 10.



Out-of-plane displacement

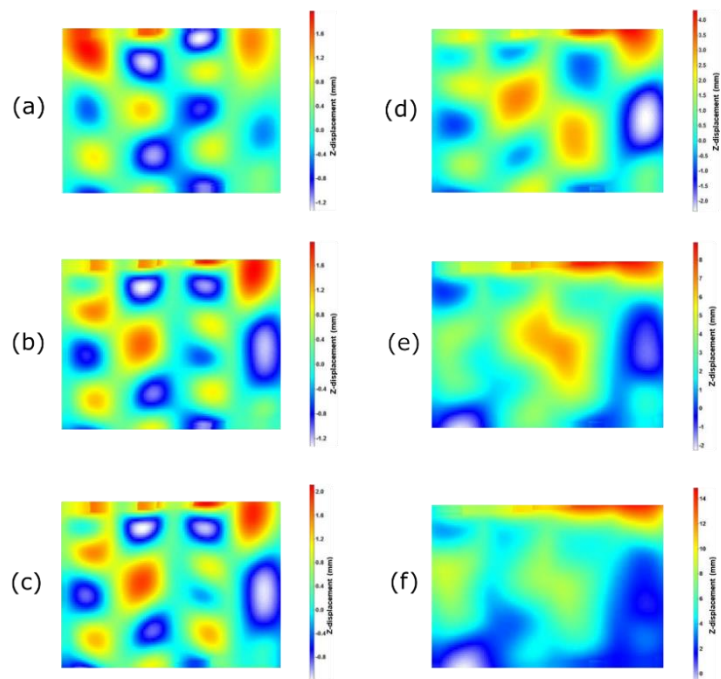


Figure 8: Experimental tests: flat panel 1 force-displacement curve and DIC out-of-plane displacement.

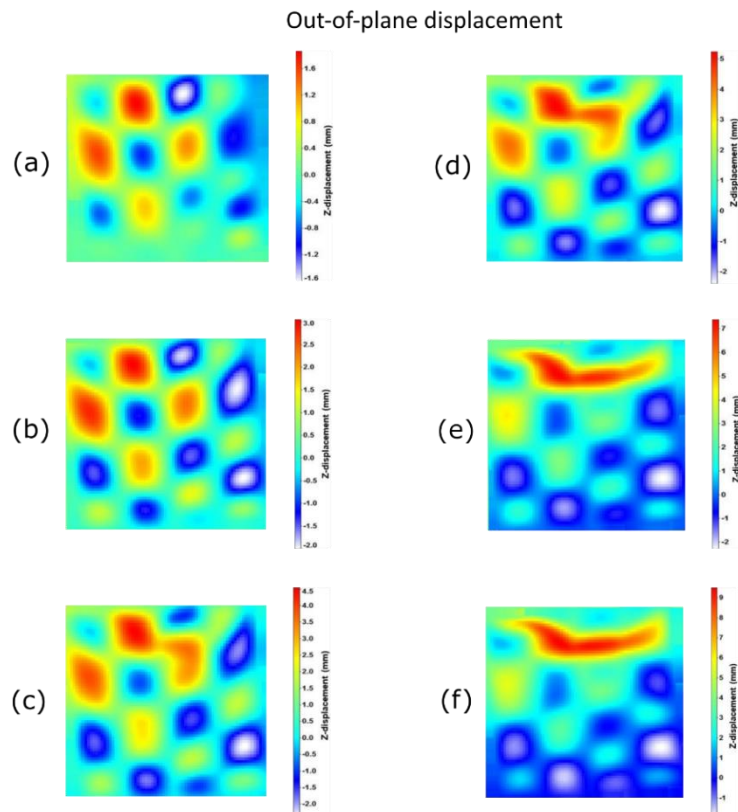
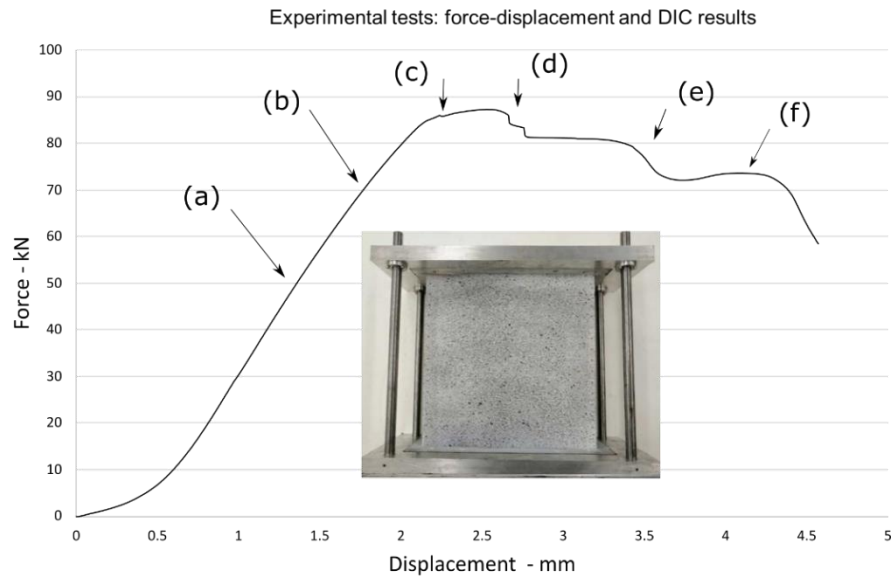


Figure 9: Experimental tests: flat panel 2 force-displacement curve and DIC out-of-plane displacement.

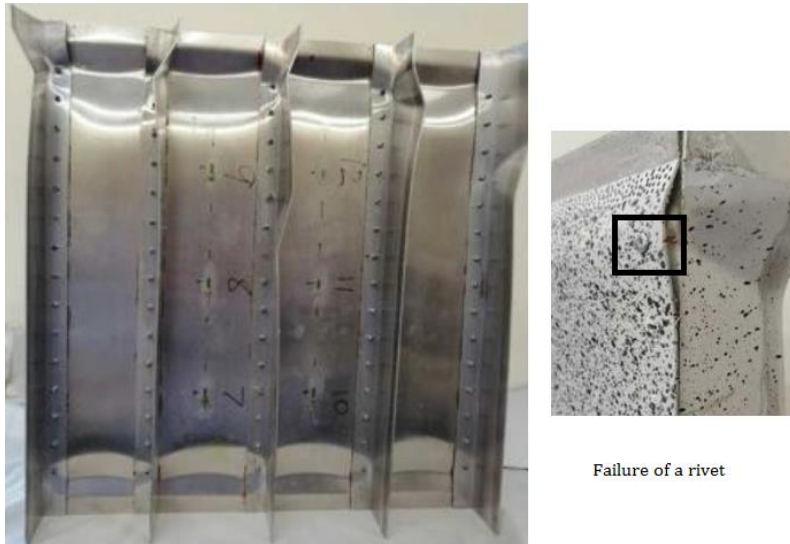


Figure 10: Experimental tests: Panel 1 failure.

Numerical model

For the multi-component FE model, with both in-plane and out-of-plane geometric imperfections modelled, the force-displacement curve, Figure 11, shows that, following an initial linear elastic response, a maximum force of 90.5 kN is reached. Following this peak, the non-linear relationship continues with the load decreasing as both the skin and the stiffeners deform, mode jumping occurs and damage progresses in the structure.

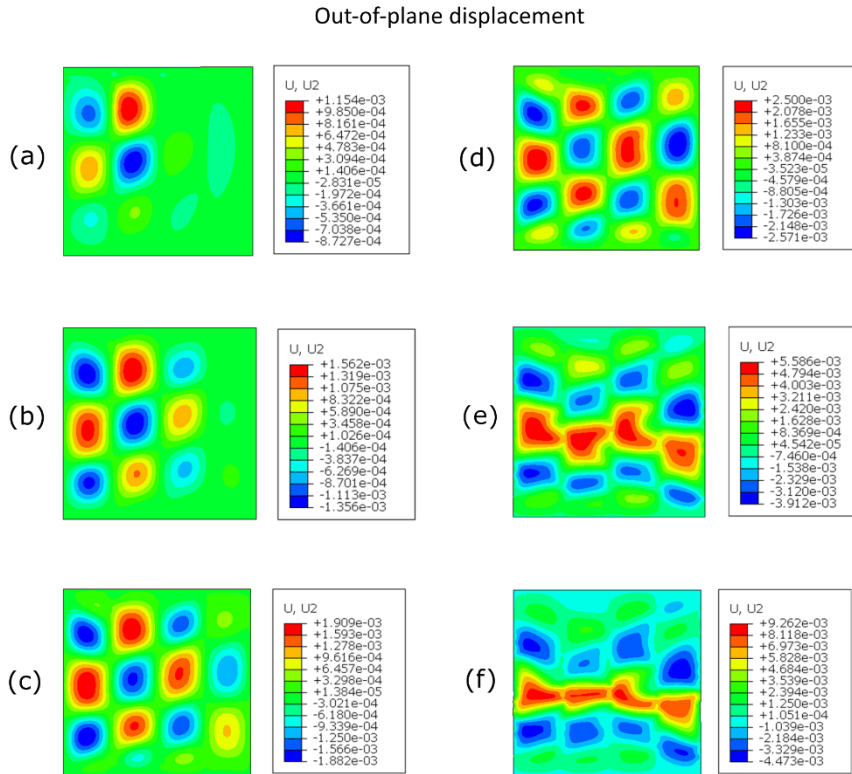
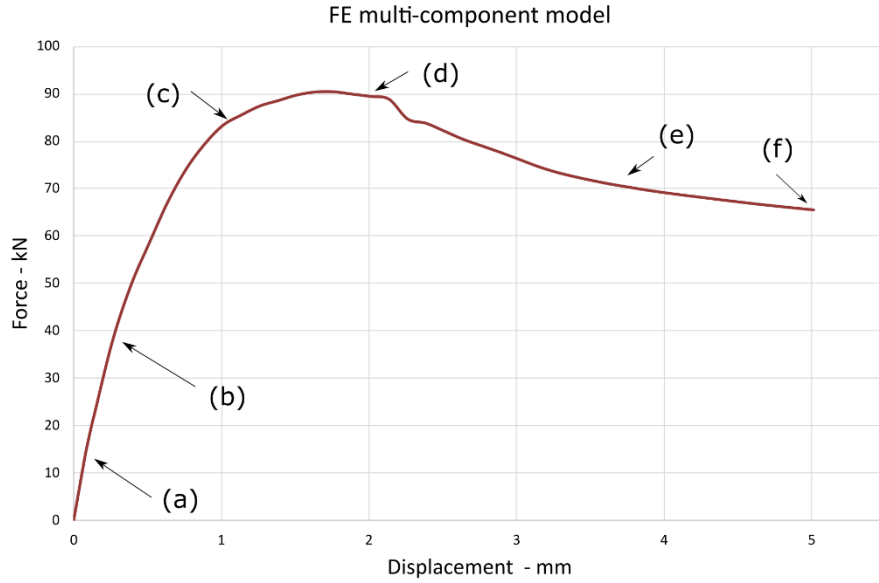


Figure 11: FE multi-component complete model: force-displacement curve and Abaqus out-of-plane displacement.

The maximum out of plane displacement predicted by the model is equal to 9.3 mm, a value that is in accordance with the range of results achieved during the experimental test results (15 mm maximum out of plane displacement for Panel 1 and 9.5 mm for Panel 2). Figure 11 indicates a buckle similar to that found experimentally, extending across the supported areas around the stiffeners as individual buckles join together. The location of this deformation differs slightly between the experimental tests and the FE model due to the fact that the out-of-plane imperfections are idealised, created as they are from superimposed eigenmodes, rather than providing an exact replication of the panel itself. However, a good agreement in out of plane response and global structural response is shown.

Discussion

Experimental-numerical comparison of results

Comparison of the experimental and numerical force-displacement curves shows similarities in the maximum load carried and post-buckling performance, as shown in Figure 12. Here, the FE force-displacement results are translated by 1 mm laterally with respect to the original experimental data for two reasons:

- To make a better comparison of the non-linear response and the peak of force
- To account for the effects of the specimen settling into the clamping system at the beginning of the tests that is not possible to replicate accurately in the FE models

Good agreement is seen in the out-of-plane displacements, comparing the DIC results and the ABAQUS model, as seen in Figures 8, 9 and 11.

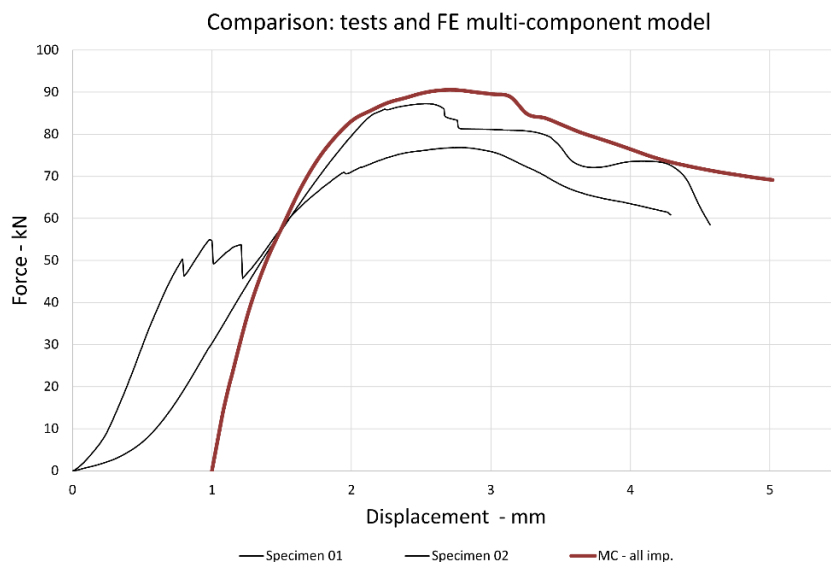


Figure 12: Comparison: experimental tests and FE model of the multi-component structure with both in-plane and out-of-plane geometric imperfections.

Effect of imperfections

The FE model with joints presented in Figure 11 refers, as mentioned above, to the multi-component stiffened structure in which all imperfections are considered. A parametric study on the effect of the presence of each single in-plane geometrical imperfection in the stiffeners, as discussed in Section 2.3, is shown in Figure 13. The benchmark used in this analysis is the multi-component model with no geometrical imperfections.

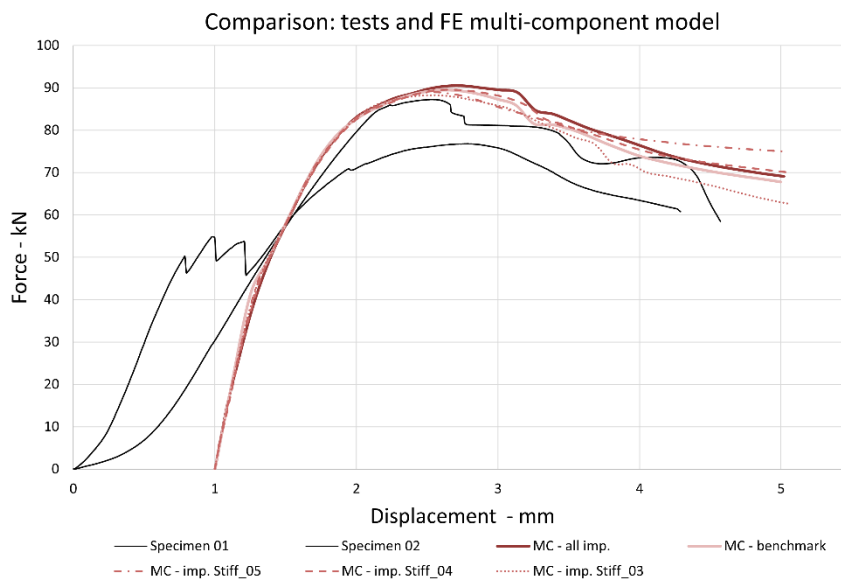


Figure 13: Comparison: experimental tests and FE model of the multi-component structure with different geometrical imperfections.

It is possible to notice that small differences between models with different imperfections introduced prior to buckling increase in the post-buckling region, higher in case all the imperfections are introduced. In both the 'benchmark' and the 'all imperfections', models, a jump in the force is visible after the peak force. Minor differences occurred in the initial linear response.

Effect of joints

As well as the geometric imperfections, the presence of the joints strongly affects the structural response. In analogy with the multi-component model, a parametric study based on the use of different localised geometrical imperfections, difference in stiffeners' length, is presented also for the single-component model, Figure 14. The single-component FE models, as shown in Figure 14, have a significantly extended the linear elastic region when compared to the multi-component models since removing component interaction leads to a reduction in initial contacts and hence localised deformation. In the post-buckling region, a very different trend is seen in the 'all imperfections' and

'benchmark' cases. For the 'all imperfections' model, the force-displacement curve decreases, following a similar trend to that shown by the multi-component model, although at a significantly higher load. The 'benchmark' case, on the other hand, shows an additional increment in force with a peak around 128 kN prior to a progressive decrease in load. These observations clearly show that the presence of discrete elements simulating the rivets in the joints affect the global behaviour of the structure, leading to a structural response much closer to the experimental one.

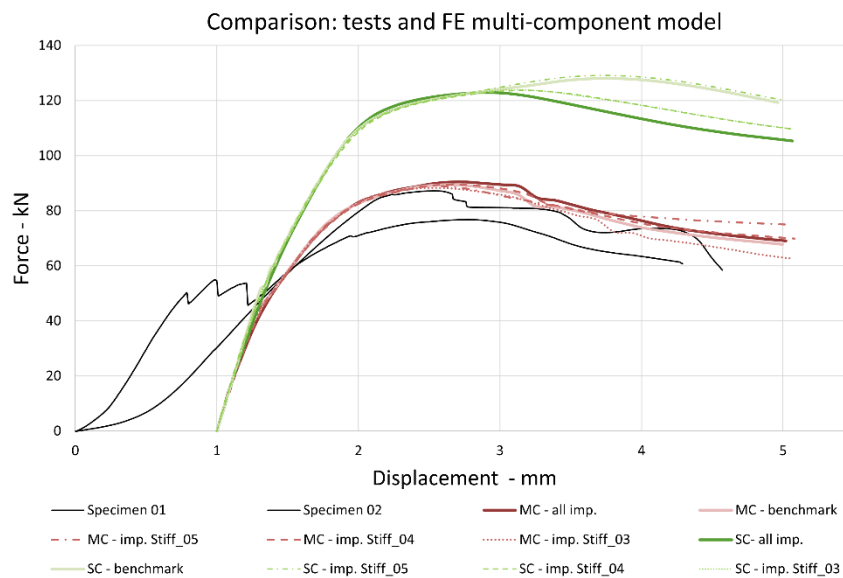


Figure 14: Comparison: experimental tests and FE model of the single-component and multi-component structures with different geometrical imperfections.

Conclusions

Manufacturing stiffened structures can lead to the presence of small imperfections such as misalignments (e.g. the ends of the components do not line up), non-uniform joint locations (e.g. non-uniform joint spans and positioning on the structure) or non-orthogonal placement with respect to the structures connected. For many years, researchers have known that these imperfections can strongly affect response especially in thin-walled structures.

In this research activity, experimental tests and FE models of a stiffened panel in which the stiffeners are connected using rivets are proposed. From the results, differences in force-displacement behaviour in the experimental tests have been attributed to premature localised damage, due to the presence of imperfections in the structure. When a single-component FE model was used however, even with geometric imperfections introduced, agreement with experimental results

was found to be poor due to the reduced component interaction causing a higher load to be carried and a difference in post-buckling behaviour. By introducing a more representative joint model correspondence between experimental and numerical results has been shown to be significantly improved. In both cases, the introduction of geometric imperfections can be seen to affect the post-buckling behaviour significantly. Thus, the use of a representative joint model is seen to be the most significant factor in developing accurate models of the buckling and post buckling of stiffened panels although geometric imperfections are important particularly in the post buckling region. Further improvements to the modelling of joints such as the introduction of plasticity and a failure criterion into the model of the rivets would therefore be worthwhile although these would be at increased computational cost.

The importance of the joint in the behaviour of stiffened panels highlights the likely improvement which could be gained from techniques such as additive manufacturing where panels are generated as one part without the wastage associated with machining from solid.

Acknowledgements

The authors would like to thank the EPSRC Research Grant Engineering Fellowships for Growth: Materials by Design for Impact in Aerospace Engineering (EPSRC Grant EP/M002322/2) and the Higher Committee for Education Development in Iraq for funding the research activity of Dr Al-Saymaree.

An additional thanks to all the technical staff of the Civil/Structural and Mechanical Laboratory of Cardiff University, Engineering Department and the IT service for their help.

Affiliation

Dr Al-Saymaree has recently moved to the College of Engineering, University of Basrah, Basra, Iraq.

References

- [1] V.O. Balabanov, R.T. Haftka, Topology optimization of transport wing internal structure, *Journal of Aircraft* 33(1) (1996) 232. <https://doi.org/10.2514/3.46926>
- [2] P.D. Dunning, B.K. Stanford, H.A. Kim, Aerostructural level set topology optimization for a common research model wing, 10th AIAA Multidisciplinary Design Optimization Conference, Maryland, USA (2014). <https://doi.org/10.2514/6.2014-0634>
- [3] N. Aage, E. Andreassen, B.S. Lazarov, O. Sigmund, Giga-voxel computational morphogenesis for structural design. *Nature*, 550 (2017) 84–86. <https://doi.org/10.1038/nature23911>

- [4] C.A. Featherston, Smart meshing of imperfect structures for the improved prediction of buckling and postbuckling behaviour. 13th International Conference on Experimental Mechanics, Alexandroupolis, Greece (2007).
- [5] R.J. Mania, A. Madeo, G. Zucco, T. Kubiak, Imperfection sensitivity of post-buckling of FML channel section column, *Thin-Walled Structures*, 114 (2017) 32-38. <https://doi.org/10.1016/j.tws.2017.01.033>
- [6] L.A. Godoy, *Thin-Walled Structures with Imperfections: Analysis and Behaviour*, Oxford: Pergamon (1996). ISBN : 0080422667
- [7] J. Arbocz, J.M.A.M. Hol, Collapse of axially compressed cylindrical shells with random imperfections, *AIAA Journal*, 29 (1991) 2247-2256. <https://doi.org/10.2514/3.10866>
- [8] D. Conrado da Silva, M. Vicente Donadon, M. Andrés Arbelo, A semi-analytical model for shear buckling analysis of stiffened composite panel with debonding defect, in press (2021), <https://doi.org/10.1016/j.tws.2021.108636>
- [9] A. Alhajahmad, C. Mittelstedt, Minimum weight design of curvilinearly grid-stiffened variable-stiffness composite fuselage panels considering buckling and manufacturing constraints, 161 (2021) <https://doi.org/10.1016/j.tws.2021.107526>
- [10] X. Kong, Y. Yang, J. Gan, T. Yuan, L. Ao, W. Wu, Experimental and numerical investigation on the detailed buckling process of similar stiffened panels subjected to in-plane compressive load, *Thin-Walled Structures*, 148 (2020) 106620. <https://doi.org/10.1016/j.tws.2020.106620>
- [11] F. Ljubinković, J.P. Martins, H. Gervásio, L. Simões da Silva, C. Leitão, Experimental and numerical investigation on cylindrically curved steel panels under uniform compression, *Thin-Walled Structures*, 149 (2020) 106527. <https://doi.org/10.1016/j.tws.2019.106527>
- [12] J.P. Martins, F. Ljubinkovic, L. Simões da Silva, H. Gervásio, of thin-walled curved steel plates under generalised in-plane stresses: a review, *Journal of Constructional Steel Research*, 140 (2018) 191-207. <https://doi.org/10.1016/j.jcsr.2017.10.018>
- [13] T. Manco, J.P. Martins, C. Rigueiro, L. Simões da Silva, Ultimate resistance of isotropic cylindrically curved steel panels under uniaxial compression, *Journal of Constructional Steel Research*, 159 (2019) 95-108. <https://doi.org/10.1016/j.jcsr.2019.04.026>
- [14] F. Goncalves Garcia, R. Ramos Jr, Design charts for the local buckling analysis of integrally web-stiffened panels with filleted junctions subjected to uniaxial compressive loads, in press (2021) <https://doi.org/10.1016/j.tws.2021.108632>
- [15] A.N.P. Andico, Y.-M . Park, B.H. Choi, Buckling strength increment of curved panels due to rotational stiffness of closed-section ribs under uniaxial compression, *International Journal of Steel Structures*, 18 (2018), 1363-1372. <https://doi.org/10.1007/s13296-018-0141-8>

- [16] K.L. Tran, C. Douthe, K. Sab, J. Dallot, L. Davaine, Buckling of stiffened curved panels under uniform axial compression, *Journal of Constructional Steel Research*, 103 (2014) 140-147. <https://doi.org/10.1016/j.jcsr.2014.07.004>
- [17] M.C. Xu, C. Guedes Soares, Comparisons of calculations with experiments on the ultimate strength of wide stiffened panels, *Marine Structures*, 31 (2013) 82-101. <https://doi.org/10.1016/j.marstruc.2013.01.003>
- [18] X.H. Shi, J. Zhang, C. Guedes Soares, Numerical assessment of experiments on the residual ultimate strength of stiffened plates with a crack, *Ocean Engineering*, 171 (2019) 443-457. <https://doi.org/10.1016/j.oceaneng.2018.10.043>
- [19] M.C. Xu, D. Yanagihara, M. Fujikubo, C. Guedes Soares, Influence of boundary conditions on the collapse behaviour of stiffened panels under combined loads, *Marine Structures*, 34 (2013) 205-225. <https://doi.org/10.1016/j.marstruc.2013.09.002>
- [20] LaVision Digital Image Correlation (DIC) systems. Online at: <http://www.lavision.de/en/>
- [21] British Standard BS EN ISO 6892-1:2016, Metallic materials — Tensile Testing Part 1: Method of test at room temperature (ISO 6892-1:2016), BSI Standard Publications, (2016). ISBN 9780580800993
- [22] Dartec mechanical testing machine. Online at: <https://www.cardiff.ac.uk/engineering/research/facilities/structural-performance-laboratory>
- [23] AALCO. 2017. Aluminium Alloy - Commercial Alloy - 6082 - T6-T651 Plate. Available at www.aalco.co.uk/datasheets/Aluminium-Alloy_6082-T6~T651_148.ashx [Accessed 22nd January 2020], Aalco Material Datasheet, 2020.
- [24] Al 6082-T6 datasheet, available online at: https://www.wilsonsmetals.com/datasheets/view/Aluminium-Alloy-6082-T6T651-Plate_148 (2020)
- [25] Loctite Multi/Bond 330 adhesive. Technical Datasheet online at: https://uk.rs-online.com/web/p/adhesives/0108738/?cm_mmc=UK-PPC-DS3A-_-bing-_-2_UK_EN_LS_Loctite_Exact_-Loctite%7CAcrylic_Adhesives-_-loctite%20330%20adhesive&gclid=0c0b792fda35137fb6be195aaf58f513&gclid=3p.ds&kwd=71811997165473%3Aloc-188&matchtype=e&mclid=0c0b792fda35137fb6be195aaf58f513&s_kwid=AL!7457!3!!e!!s!!loctite%20330%20adhesive&utm_campaign=2_UK_EN_LS_Loctite_Exact&utm_content=Loctite%7CAcrylic_Adhesives&utm_medium=cpc&utm_source=bing&utm_term=loctite%20330%20adhesive
- [26] M.L. Longana, Intermediate Strain Rate Testing Methodologies and Full-Field Optical Strain Measurement Techniques for Composite Materials Characterisation, PhD thesis, University of Southampton, Faculty of Engineering and the Environment (2014).

- [27] A. Prato, M.L. Longana, A. Hussain, M.R. Wisnom, Post-impact behaviour of pseudo-ductile thin-ply angle-ply hybrid composites, *Materials*, MDPI, 12(4) (2019) 579. <https://doi.org/10.3390/ma12040579>
- [28] A. Prato, M.L. Longana, A novel approach for the investigation of low energy ice impacts, *Journal of Impact Engineering*, 121 (2018) 12-19. <https://doi.org/10.1016/j.ijimpeng.2018.06.003>
- [29] Dassault Systems, ABAQUS Unified FEA. Online at: <https://www.3ds.com/products-services/simulia/products/abaqus/>
- [30] Dassault Systemes Simulia Corp., SIMULIA User Assistance 2017, ABAQUS User's Guide, manual linked to the software.
- [31] M.S.M. Al-Saymaree, Exact Strip Analysis and Experiments on Buckling and Post-buckling of Plates and Stiffened Panels with Mode Jumping, PhD thesis, Cardiff University, School of Engineering, Cardiff, UK (2019).